

Cryogenic formation-structure-property relationships of poly(2-acrylamido-2-methyl-1-propanesulfonic acid) cryogels

Esra Su, Oguz Okay*

Department of Chemistry, Istanbul Technical University, 34469, Maslak, Istanbul, Turkey



HIGHLIGHTS

- Macroporous AMPS cryogels are prepared in aqueous solutions at -18°C .
- Local conditions of the gelation system determine the cryogel properties.
- Young's modulus and fracture stress of the cryogels are 0.73 and 6 MPa, respectively.
- They are completely squeezable under strain, and exhibit superfast responsivity.

ARTICLE INFO

Keywords:

Cryogelation
2-Acrylamido-2-methyl-1-propanesulfonic acid
Macroporous hydrogels

ABSTRACT

Cryogelation is a simple and eco-friendly technique to produce macroporous cryogels exhibiting extraordinary mechanical properties. Most of the results on cryogels reported so far, however, lack a more detailed analysis to provide real conditions of the cryogelation system, which is an apparently frozen reaction solution. We investigate here the correlations between the cryogelation conditions and properties of poly(2-acrylamido-2-methyl-1-propanesulfonic acid) (PAMPS) cryogels, which are attractive materials with a wide range of application areas. PAMPS cryogels are prepared by free-radical copolymerization of AMPS and *N,N'*-methylenebis(acrylamide) (BAAm) in aqueous solutions at -18°C in the presence of a redox initiator system. The total pore volume of the cryogels decreases whereas the average pore diameter increases with increasing AMPS concentration C_0 . The morphological variations depending on C_0 could be explained with the local conditions during cryogelation, i.e., the melting temperature of the reaction solution, the ice volume, and the true concentration of the monomers in unfrozen domains. PAMPS cryogels prepared at 9.1 mol % BAAm exhibit the highest modulus (0.73 ± 0.05 MPa) and could withstand up to 6.0 ± 0.5 MPa compressive fracture stress.

1. Introduction

Hydrogels based on 2-acrylamido-2-methyl-1-propanesulfonic acid (AMPS) attract significant interest in the past decades due to their strong polyelectrolyte behavior that provides a pH-independent large water uptake capacity [1–6]. Poly(AMPS) (PAMPS) hydrogels have various potential application areas for the use in water purification, food industry, agriculture, energy and environmental fields, and bioengineering [7–12]. PAMPS hydrogels with a covalently cross-linked network structure have generally been prepared via free-radical cross-linking copolymerization of AMPS and a divinyl monomer, typically *N,N'*-methylenebis(acrylamide) (BAAm) in aqueous solutions [4]. Such hydrogels exhibit, however, insufficient mechanical performances restricting their applications.

An alternative strategy to generate PAMPS hydrogels is the

cryogelation technique which is a simple and eco-friendly technique to produce macroporous hydrogels, so-called cryogels [13–17]. Cryogelation bases on conducting the gelation reactions in an apparently frozen reaction system. By this technique, free-radical cross-linking copolymerization reactions are generally conducted in aqueous media below the freezing temperature of the reaction system. As water freezes, monomers expelled from the ice concentrate in the unfrozen domains making them a highly concentrated solution, which is called cryoconcentration [13,15,16]. After attaining thermal equilibrium with the surrounding cold bath, the reaction system consists of unfrozen solution phase containing a high concentration of monomers and initiator, interconnected by ice crystals. Because the cryoconcentration effect generally dominates over the reduced polymerization rates due to the low temperature, cryogels can be obtained even at very low concentration [15,18]. After cryogelation followed by thawing the ice

* Corresponding author.

E-mail address: okayoy@itu.edu.tr (O. Okay).

crystals acting as a template for the pores, a 3D network of polymers containing μm -sized pores is obtained.

It is worth to mention that the cryoconcentration is a characteristic phenomenon of cryogelation, which distinguishes it from freeze-drying. For instance, freeze-drying of an already formed hydrogel does not lead to materials with cryogel properties due to the formation of ice crystals in a gel network rather than in a solution [15]. The pore wall produced by cryogelation is a dense polymeric gel because of the cryoconcentrated solution of the monomers around the ice crystals. In contrast, the pore wall formed after freeze-drying of a conventional hydrogel is a loosely cross-linked gel due to the absence of cryoconcentration. As a consequence, the porous structures produced during cryogelation are mechanically stable, even under large strain conditions, whereas those produced during freeze-drying are generally brittle in nature. For instance, it was shown that the cryogel scaffolds prepared from frozen aqueous silk fibroin solutions at -18°C exhibit a Young's modulus of 8 MPa and a compressive fracture stress of 0.22 MPa, which are about 1 order of magnitude higher than those of the corresponding freeze-dried fibroin hydrogels prepared at 50°C [19].

Thus, cryogelation leads to a significant change in the mechanical performances of the classical first-generation hydrogels. Almost complete squeezability, high-toughness, and superfast responsivity are some of the characteristics of the cryogels which are not observed in the hydrogels [15,19]. Most of the results on cryogels reported so far, however, lack a more detailed analysis to provide real conditions of the cryogelation systems. This includes the true concentration of the monomers in the unfrozen domains during cryogelation and its variation depending on the nominal monomer concentration. We investigate here the correlations between the properties of PAMPS cryogels including their porous structures and mechanical performances with the cryogelation conditions. We prepare PAMPS cryogels from aqueous solutions of AMPS and BAAM at various concentrations in the presence of a redox initiator system at -18°C . As will be seen below, a clear correlation was found between the morphology of the cryogels and the local conditions during cryogelation including the melting temperature of the reaction solution, the volume of ice template, and the true concentration of the monomers in unfrozen domains. We also show a significant improvement in the mechanical properties of the cryogels with increasing BAAM content. PAMPS cryogels prepared at 9.1 mol % BAAM exhibit the highest modulus (0.73 ± 0.05 MPa) and could withstand up to 6.0 ± 0.5 MPa compressive fracture stress.

2. Experimental

2.1. Materials

2-Acrylamido-2-methylpropane sulfonic acid (AMPS, Merck), N, N'-methylenebis(acrylamide) (BAAM, Merck), potassium persulfate (KPS, Merck), N, N, N', N'-tetramethylethylenediamine (TEMED, Merck), and sodium hydroxide (NaOH, Merck) were used as received. To prepare 0.966 M aqueous solution of sodium salt of AMPS (AMPS-Na), AMPS (20 g) was first dissolved in 40 mL distilled water at $23 \pm 2^\circ\text{C}$ under stirring. After addition of 10 mL of 30 w/v % aqueous NaOH, the solution was titrated with 1 M NaOH to pH = 7 and then, the final solution volume was completed to 100 mL with distilled water. For the preparation of the cryogels at a monomer concentration of 24 wt %, 1.18 M aqueous AMPS-Na solution was prepared starting from 24.33 g AMPS. 24 mM KPS stock solution was prepared by dissolving 65 mg KPS in 10 mL distilled water.

2.2. Cryogel preparation

PAMPS cryogels were prepared from aqueous solutions of AMPS-Na and BAAM at -18°C in the presence of 1 mol % KPS (with respect to the monomers) and 0.25 v/v % TEMED as a redox initiator system. To prevent the onset of gelation before freezing of the reaction solution at

-18°C , the solutions were pre-cooled at -196°C . Two sets of experiments were carried out. In the first set, BAAM content in the monomer feed was varied between 1.2 and 9.1 mol % at a total monomer concentration C_o of 10 wt % whereas in the second set, C_o was changed between 10 and 25 wt % at 1.2 mol % BAAM. A typical synthetic procedure for the preparation of the cryogels at $C_o = 15$ wt % and 1.2 mol % BAAM follows: BAAM (14 mg) was dissolved in 6.2 mL of 0.966 M AMPS-Na stock solution and the volume of the solution was completed to 7.0 mL with distilled water. After addition of 3 mL KPS stock solution, it was cooled to 0°C in an ice bath and bubbled nitrogen for 10 min to remove oxygen, TEMED (25 μL) was then added and the solution was transferred into plastic 1 mL-syringes. The syringes were first immersed into liquid nitrogen for 2 min and then transferred into a cryostat at -18°C to conduct the cryogelation reactions for 24 h.

2.3. Determination of unfrozen water content during cryogelation

The amount of unfrozen water during cryogelation and true monomer concentration in the unfrozen domains were estimated by differential scanning calorimetry (DSC). For this purpose, gelation solutions containing various amounts of AMPS-Na and BAAM were prepared as described above, except that KPS-TEMED initiator system was not included. The solutions in the plastic syringes were immersed into liquid nitrogen for 2 min followed into a cryostat at -18°C for 24 h. 30 mg of the frozen solution was then transferred in an aluminum pan of the instrument (Perkin-Elmer Diamond DSC). After sealing and weighing of the pan, the solution was frozen within the instrument at -18°C for 2 h and then heated from 10°C with a scanning rate of 1°C min^{-1} . From the melting enthalpy ΔH of frozen water, the mass fraction f_{unf} of unfrozen water in the apparently frozen solution at -18°C was calculated as

$$f_{unf} = 1 - \frac{\Delta H}{\Delta H_m} \quad (1)$$

where ΔH_m is the melting enthalpy of ice (6.01 kJ mol^{-1}).

2.4. Characterization of cryogels

PAMPS cryogels taken out of the syringes after a reaction time of 24 h were cut into small pieces of about 1 cm in length and they were immersed in an excess of water at room temperature to remove soluble species. After reaching equilibrium degree of swelling, which was monitored by recording the mass and the diameter of the gel specimens, they were freeze-dried (Christ Alpha 2e4 LD-plus) for 2 days. The gel fraction W_g , i.e., the fraction of cross-linked polymer obtained from 1 g of AMPS was calculated as

$$W_g = \frac{m_{dry}}{m_o w_{AMPS}} \quad (2)$$

where m_{dry} and m_o are the weights of the gel specimens in dried and as-prepared states, respectively, w_{AMPS} is the weight fraction of AMPS in the initial reaction solution. The equilibrium weight q_w and volume swelling ratios q_v of the cryogels in water were calculated as

$$q_w = \frac{m_s}{m_{dry}} \quad (3)$$

$$q_v = \left(\frac{D_s}{D_{dry}} \right)^3 \quad (4)$$

where D_{dry} and m_{dry} are the diameter and mass of the specimens in dried state, respectively, and D_s and m_s are the same quantities but of the equilibrium swollen specimens. To determine the pore volume V_p of the cryogels, dried gel specimens were immersed in an excess of acetone and their equilibrium masses m_{Ace} were recorded. The pore volume V_p , that is, the total volume of the pores in unit mass of dry PAMPS network was estimated using the equation,

$$V_p = \frac{m_{Ace} - m_{dry}}{d_{Ace} m_{dry}} \quad (5)$$

where d_{Ace} is the density of acetone (0.784 g mL^{-1}).

For the texture determination of dried cryogels, scanning electron microscopy (SEM) measurements were carried out at various magnifications on Tescan GAIA 3 Field Emission SEM. Prior to the measurements, the specimens were sputter-coated with gold-palladium using Leica ACE 600 instrument. The average pore diameters D were calculated from at least 10 SEM images taken at various magnifications using ImageJ image processing software (US National Institutes of Health, Bethesda, MD).

The morphology of the cryogels was also visualized using micro-computed tomography (μ -CT) scanning performed using a μ -CT Skyscan 1272 instrument (Bruker, Belgium) working at a voltage of 55 kV and a current of 53 μ A. All gel specimens were scanned at a 15.3 μ m pixel resolution and 180° rotation around their vertical axes, with 2 average frames at every 0.20 angle step. The integration time was set to 70 ms and no filter was applied. Reconstructions were carried out using NRecon 1.7.4.2 reconstruction software (Skyscan, Bruker, Belgium) using a full cone beam Feldkamp reconstruction algorithm with grayscale limits defined automatically. Reconstructed data were further processed in the volume of interest (VOI) data-sets within CTAn 1.18.4.0 + software (Skyscan, Bruker, Belgium) to investigate pore sizes, structure wall thickness, and porosity. To produce binary images for the morphological characterization of the cryogels, thresholding by hysteresis was used as the segmentation method. An optimal threshold for each analysis was chosen and kept consistent throughout all evaluations. To visualize the cryogel samples, reconstructed images were volume-rendered within CTVOx 3.3.0 r1403 program (Skyscan, Bruker, Belgium).

Uniaxial compression tests were performed on cylindrical gel specimens at $23 \pm 2^\circ \text{C}$ on a Zwick Roell mechanical test machine using 500 N load cell at a strain rate of 50 mm/min. The stress was calculated as its nominal σ_{nom} value which is the force per cross-sectional area of undeformed specimen, while the strain was given by the elongation ratio ϵ . Young's modulus E was calculated from the slope of stress-strain curves between 5 and 10% elongation. The compressive fracture stress and strain were calculated from the maxima of true stress-strain curves as detailed before [20].

3. Results and discussion

PAMPS cryogels were prepared from aqueous solutions of AMPS-Na and BAAM at -18°C in the presence of KPS-TEMED redox initiator system. To highlight the individual effects of the monomer AMPS-Na and the cross-linker BAAM on the cryogel properties, two sets of experiments were carried out: In the first set, BAAM content was varied between 1.2 and 9.1 mol % at a total monomer (AMPS-Na + BAAM) concentration C_o of 10 wt %. In the second set, C_o was varied between 10 and 25 wt % at a fixed BAAM content of 1.2 mol %. Gel fraction measurements showed that all cryogels reported here exhibit a gel fraction close to unity after a reaction time of 24 h (Figure S1), indicating that the monomers in the feed are completely incorporated into the cryogel network.

Fig. 1a shows typical optical images of the cryogels at $23 \pm 2^\circ \text{C}$ formed at various monomer concentrations C_o in swollen (upper panel) and dried states (bottom panel). At $C_o < 20 \text{ wt } \%$, swollen cryogels are transparent due to their high water contents (98–99%) whereas those produced at higher concentrations are translucent revealing scattering of light from separate domains. They all become opaque in their dried states reflecting their macroporous structures. Moreover, all cryogels reported here exhibit superfast swelling response when immersed in a good solvent. For instance, Fig. 1b shows the images of a cryogel specimen before (1) and just after immersion in water colored with crystal violet (2). The specimen immediately absorbs the solution to attain its

equilibrium swollen state and exhibits a blue-violet color which is the typical color of crystal violet (CV) at a neutral pH. After a waiting time of 1 h, the color of the cryogel turns to green corresponding to a form of CV with two of the nitrogen atoms positively charged due to the acidic character of PAMPS (images 3, 4 in Fig. 1b). Thus, swelling of dry gel specimen occurs faster than the chemical equilibration of CV with the gel phase.

Fig. 2a shows the equilibrium weight q_w and volume swelling ratios q_v of PAMPS cryogels in water as functions of BAAM (circles) and monomer concentrations C_o (triangles). The cryogels exhibit a large weight swelling ratio q_w between 70 and 20, which is a decreasing function of both the cross-linker or monomer concentrations. The volume swelling ratios q_v are 14- to 44-fold smaller than q_w 's, and slight increasing functions of BAAM % and C_o . Because the volume swelling is mainly determined by the expansion of the 3D PAMPS network in water due to the favorable PAMPS–water interactions while weight swelling also includes filling of the micro-voids within the gel with the solvent, this finding reflects the existence of an interconnected open porous structure in PAMPS cryogels. The total pore volume of the cryogels was estimated from the uptake of acetone, which is a poor solvent of PAMPS and hence, preferentially enters the open pores of the cryogels. We found that the total pore volume V_p is independent of BAAM % within the limits of the experimental error, i.e., $2.4 \pm 0.4 \text{ mL g}^{-1}$, whereas it decreases from 2.6 to 1.3 mL g^{-1} as the monomer concentration C_o is increased (Fig. 2b). This behavior is attributed to the decreasing amount of water in the gelation solution as C_o is increased leading to the formation of a lesser amount of ice acting as a template for the formation of pores.

To determine the morphology of the cryogels, we used both SEM and μ -CT techniques which are destructive and nondestructive tests, respectively, for the characterization of the porous structures. Moreover, the advantage of SEM is its higher magnification and more precise determination of the pore diameters as compared to μ -CT. Fig. 3a–c shows 3D and 2D μ -CT, and SEM images of the cryogels, respectively, at a low magnification (scaling bars = 0.5–2 mm). The cryogels were prepared at $C_o = 10$ (upper panel) and 25 wt % (bottom panel). All images show pore channels templated from the growing ice crystals during cryogelation. The channels are aligned in radial directions the extent of which slightly decreases as C_o is increased from 10 to 25 wt %. The aligned pore channels are also illustrated in the attached movie (Supporting Information movie). We attribute the alignment of the pore channels to the pre-cooling step of the reaction solution in liquid nitrogen, as illustrated in Scheme 1. Fast cooling of the solution in the cold bath at -196°C results in the rapid growth of ice from the surface of the reactor to the interior, i.e., in the direction of the temperature gradient.

μ -CT analysis also revealed the existence of less than 0.006% closed pores in the cryogels and hence, they exhibit a highly porous, interconnected open pore structure. Fig. 4 shows SEM images of the cryogels formed at various concentrations C_o at $300\times$ (upper panel) and $500\times$ magnifications (bottom panel). Aligned pore channels forming a layered structure appear at $C_o = 10$ and 15 wt %, whereas the degree of alignment decreases above 15%. Thus, in accord with μ -CT images, cryogels formed below $C_o = 20 \text{ wt } \%$ exhibit an aligned morphology. The existence of an interconnected open pore structure together with an aligned morphology is important for many application areas of macroporous materials including tissue engineering, bioseparation, microfluidics, and organic electronics [21,22]. Spherical pores within the layers together with irregular pores between the layers exist in the cryogels whose number increases with increasing concentration C_o . Moreover, both μ -CT and SEM images show no detectable effect of BAAM content on the morphology and pore size of the cryogels.

Fig. 5a shows average pore diameters (D) and distances (l) between the layers estimated from the SEM images plotted against the monomer concentration C_o . Average pore diameter slightly increases from 34 ± 7 to $50 \pm 7 \mu\text{m}$ whereas layer spacing decreases from 168 ± 23

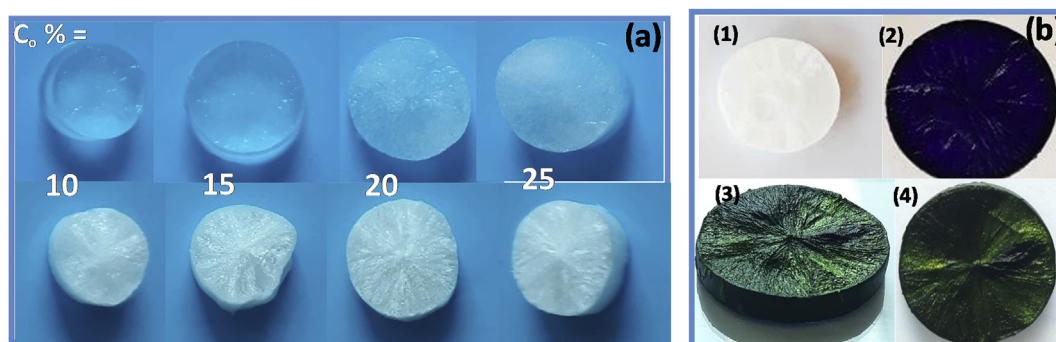


Fig. 1. (a) Optical images of PAMPS cryogel specimens formed at 1.2 mol % BAAM and at various C_0 in swollen (upper panel) and dry states (bottom panel). (b) Optical images of a cryogel specimen before (1), just after immersion in an aqueous solution of crystal violet (2), after 1 h (3) and 24 h (4). $C_0 = 10$ wt %. BAAM = 1.2 mol % BAAM. (For interpretation of the references to color in this figure legend, the reader is referred to the Web version of this article.)

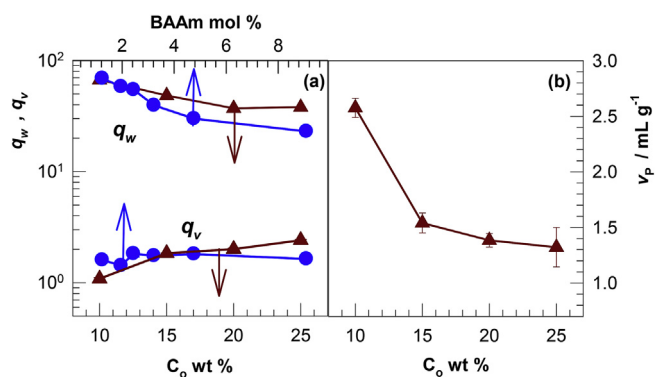
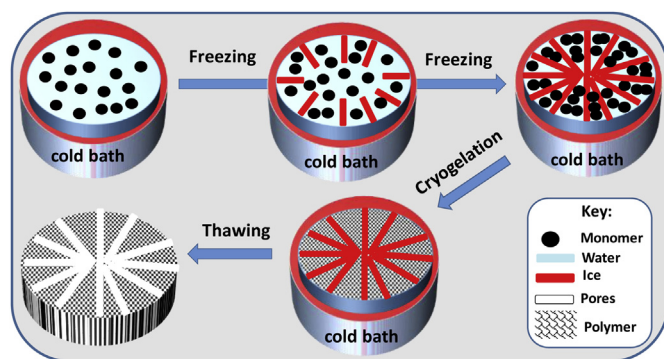


Fig. 2. Equilibrium weight q_w and volume swelling ratios q_v , (a) and pore volumes V_p (b) of PAMPS cryogels shown as functions of the monomer concentration C_0 (triangles) and BAAM content (circles).



Scheme 1. Cartoon showing cryogelation of the monomers under fast freezing condition in a radial direction from surface to the interior.

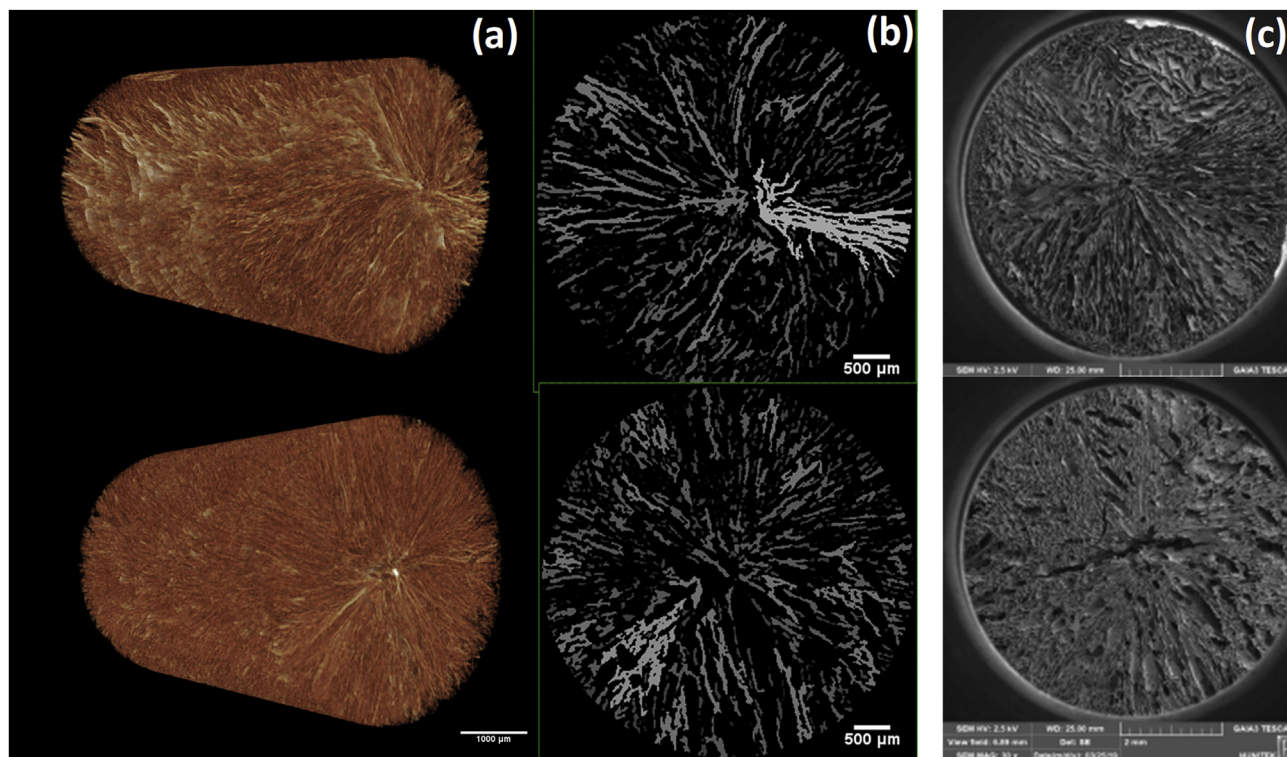


Fig. 3. 3D (a), 2D μ -CT (b), and SEM images (c) of cryogels formed at $C_0 = 10$ (upper panel) and 25 wt % (bottom panel). Scale bars are 1 (a), 0.5 (b), and 2 mm (c). BAAM = 1.2 mol %.

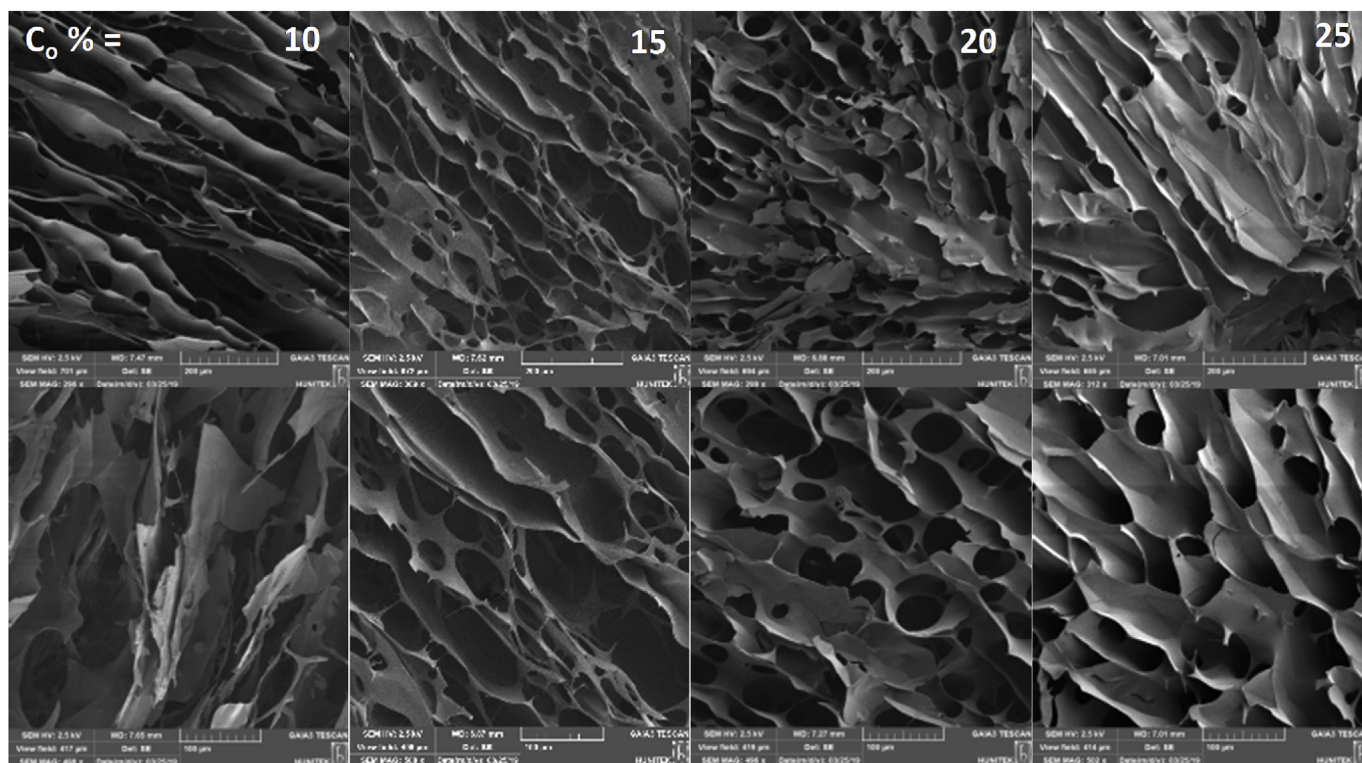


Fig. 4. SEM images of cryogels formed at various C_0 as indicated. Scale bars are 200 (upper panel) and 100 μm (bottom panel). BAAM = 1.2 mol %.

to $111 \pm 10 \mu\text{m}$ as the monomer concentration C_0 is increased from 10 to 25 wt %. Analyzing $\mu\text{-CT}$ images of the cryogels formed at $C_0 = 10$ and 25 wt % gives a similar trend but somehow larger pore diameters (Fig. 5b). The average pore diameters estimated from $\mu\text{-CT}$ are 72 ± 20 and $85 \pm 6 \mu\text{m}$ for $C_0 = 10$ and 25 wt %, respectively, together with large pores of about 0.9 mm in diameter. We should note that the pore diameters using $\mu\text{-CT}$ are estimated based on the number of pixels present in the pores. Since one pixel corresponds to $15.3 \mu\text{m}$, the pore diameters estimated here will be at least $15 \mu\text{m}$ higher than those obtained from SEM.

To explain the observed morphological variations depending on the monomer concentration C_0 , one needs to know the local concentrations of the reaction components during cryogelation, i.e., the amounts of frozen and unfrozen water at -18°C , and the actual concentration of the monomers in the unfrozen domains. To quantify the amount of unfrozen domain during the cryogelation reactions, DSC measurements were conducted by heating frozen AMPS/BAAM solutions from -18 to 10°C with a scanning rate of 1°C min^{-1} (Figure S2). Melting peak shifted to a lower temperature and the area under the peak became

smaller as C_0 is increased, reflecting lowering the melting temperature T_m of the monomer solution and decreasing amount of ice in the reaction system. Fig. 6a shows the melting temperature T_m of the monomer solutions (triangles) and the fraction f_{unf} of unfrozen water at -18°C (circles) both plotted against C_0 . The fraction f_{unf} rapidly increases from 36 ± 2 to $79 \pm 5\%$ whereas T_m decreases from -5.5 to -12.3°C with increasing C_0 from 10 to 25 wt %. Because decreasing T_m means a slower rate of freezing of water in the reaction solution, larger ice crystals will form as C_0 is increased leading to the formation of larger pores and hence, a smaller spacing between the pores [15]. Thus, the results are consistent with the experimental finding regarding C_0 -dependence of the pore diameters and the distances between pore channels in the cryogels (Fig. 5). Moreover, decreasing freezing rate of water also leads to a lesser degree of alignment of growing ice crystals, which is in accord with the SEM and $\mu\text{-CT}$ results.

The true concentration C_{true} of the monomers in the unfrozen domains and the volume of ice per gram of dry cryogel V_{ice} can be estimated from the fraction f_{unf} of unfrozen water using the equations,

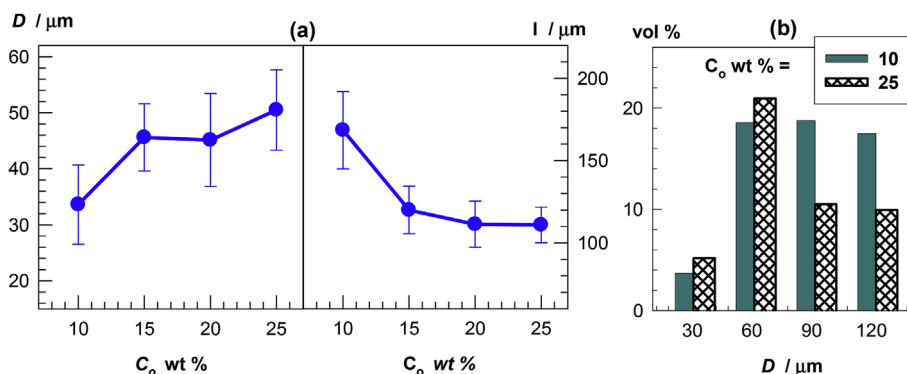


Fig. 5. (a): Average pore diameter D and layer spacing l of the cryogels calculated from the SEM images plotted against the monomer concentration C_0 . (b): Distribution of the pore diameters D estimated from $\mu\text{-CT}$ of cryogels formed at $C_0 = 10$ and 25 wt %. BAAM = 1.2 mol %.

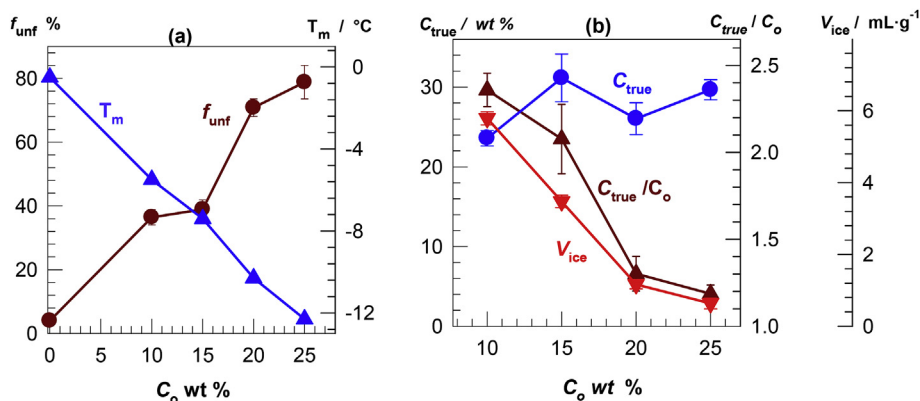


Fig. 6. (a): The fraction f_{unf} of unfrozen water at -18°C (circles) and the melting temperature T_m (triangles) both plotted against C_o . (b): True monomer concentration C_{true} in the unfrozen domains (circles), the ratio C_{true}/C_o (triangles up) and the volume V_{ice} of ice per gram of dried cryogel (triangles down) shown as a function of C_o .

$$C_{true} = \frac{10^2 C_o}{C_o + (1 - C_o) f_{unf}} \quad (6)$$

$$V_{ice} = \frac{(1 - C_o)(1 - f_{unf})}{d_1 C_o} \quad (7)$$

where d_1 is the density of ice at -18°C (0.995 g mL^{-1}). Fig. 6b shows C_{true} (circles), the ratio of true-to-nominal monomer concentration C_{true}/C_o (triangles up), and the volume of ice per gram of dry cryogel V_{ice} (triangles down) plotted against C_o . At the nominal monomer concentration C_o of 10 wt %, C_{true} is $24 \pm 1\%$ whereas, at higher concentrations, C_{true} remains constant at $29 \pm 3 \text{ wt } \%$. Thus, increasing monomer concentration in the reaction solution above 10 wt % does not change its actual concentration C_{true} in the unfrozen solution at -18°C , revealing that it is a saturated AMPS/BAAm solution. Moreover, the C_{true}/C_o ratio representing the extent of cryoconcentration is the highest at the lowest monomer concentration of 10 wt %, i.e., C_{true} is about 2.4-fold larger than C_o . Increasing C_o continuously decreases the effect of cryoconcentration and the C_{true}/C_o ratio reduces to 1.2 at $C_o = 25 \text{ wt } \%$. Fig. 6b also shows a continuous decrease of the ice volume V_{ice} with increasing C_o , which is in accord with the pore volume measurements (Fig. 2b). All these findings reveal that DSC measurements conducted on frozen gelation solutions are means for predicting the final properties of the cryogels.

Mechanical behavior of the cryogels was determined by uniaxial compression tests conducted on cryogels in their dried states at $23 \pm 2^\circ\text{C}$. Fig. 7a and b shows typical stress-strain curves of the cryogels prepared at various BAAm and monomer concentrations, respectively. The insets to the figures present the initial portion of the curves in a semi-logarithmic scale up to 23% compression. All cryogels

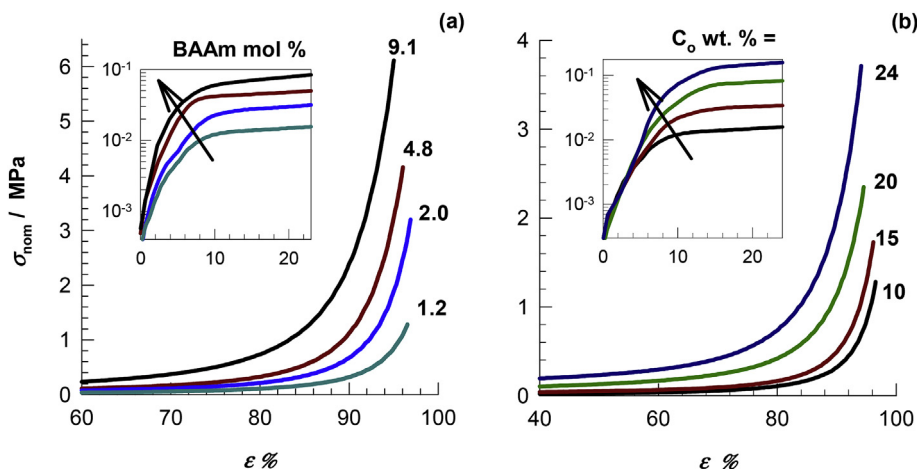


Fig. 7. Typical stress-strain curves of dried cryogels as the dependence of the nominal stress σ_{nom} on the strain ϵ . The data are from cryogels formed at various BAAm (a) and monomer concentrations C_o (b). The insets show the initial portion of the curves in a semi-logarithmic scale.

could be compressed up to 94–97% strains without any damage. Moreover, the insets reveal that the stress-strain curves first exhibit an elastic region followed by a quasi-plateau regime during which the gel specimens easily deform. Finally, they exhibit hardening behavior at strains above 80%. The appearance of a plateau regime in stress-strain curves suggests the collapse of the porous structure of the cryogels, as also reported before for silk fibroin cryogels [19]. The plateau stress increases with increasing BAAm or monomer concentration indicating increasing mechanical strength of the pore walls constituting the network structure. For instance, the plateau stress increases by one order of magnitude (from 13 kPa to 140 kPa) with increasing monomer concentration C_o from 10 to 24 w/v %.

The appearance of three regimes in the stress-strain curves was also reflected from the instantaneous slope of the stress-strain curves corresponding to the instantaneous modulus E_i of the cryogels. Fig. 8a and b shows strain-dependence of E_i of the cryogels formed at various BAAm and monomer concentrations, respectively, calculated from the slope between two consecutive data points in Fig. 7. To eliminate noise in the data series, they were smoothed using the negative exponential procedure with a sampling proportion of 0.1, i.e., 10 data points for one smoothed value (Figure S3) [23]. The modulus E_i decreases and attains a minimum value between 10 and 20% strains but then continuously increases and approaches to a value of 10^2 MPa , which is in the range of the mechanical strength of bulk polymers. This suggests the disappearance of the pores at high strains and hence compressing bulk PAMPS network. Fig. 9 shows Young's modulus E and compressive fracture stress σ_f of the cryogels plotted against BAAm and total monomer concentrations C_o . Increasing C_o or BAAm mol % also increases both Young's modulus E and compressive fracture stress σ_f of the

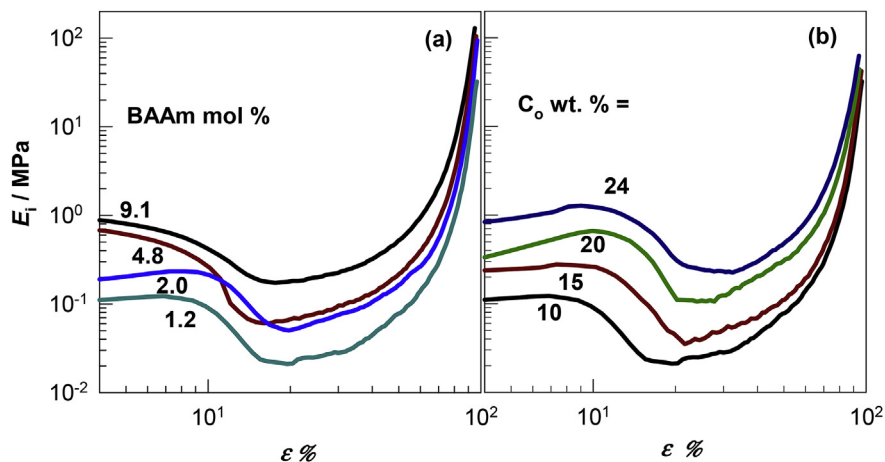


Fig. 8. Instantaneous modulus E_i of the cryogels formed at various BAAM (a) and monomer concentrations (b) plotted against the strain ϵ .

cryogels. However, a much significant improvement in the mechanical properties of the cryogels was observed at high BAAM contents. The cryogels prepared at 9.1 mol % BAAM exhibit the highest modulus (0.73 ± 0.05 MPa) and could withstand up to 6.0 ± 0.5 MPa compressive fracture stress.

All cryogels exhibited superfast swelling behavior when immersed in water (Fig. 1b). They also exhibited fast responsivity against changes in the solvent quality. Fig. 10 shows swelling-deswelling kinetics of the cryogels formed at various C_o in water and acetone, respectively, as the dependences of their weight $q_{w,t}$ and volume swelling ratios $q_{v,t}$ on the contact time t . They all attain their equilibrium swollen state in water before the first measurement time of 1 min. When equilibrium swollen cryogels are immersed in acetone, a poor solvent for PAMPS, they assume an equilibrium collapsed state within 5 min. This swelling-deswelling cycle was totally reversible and independent of BAAM content (Figure S4). Another feature of all PAMPS cryogels is their almost complete squeezability, as illustrated in Fig. 10b using the images of a colored gel specimen. Compressing the specimen under load squeezes water out of the cryogel network (images 1 \rightarrow 4) whereas, upon unloading, the specimen fully recovers its original shape by sucking back the released water into pores (images 5, 6). The cycles consisting of squeezing and autonomic reswelling steps were repeated 20 times after placing the bottom end of the specimen in contact with water. The swollen cryogels returned to their original shapes and masses after each cycle.

4. Conclusions

Cryogelation is a simple and eco-friendly technique to produce macroporous hydrogels, so-called cryogels, exhibiting extraordinary properties including large porosity, complete squeezability, high-toughness, and superfast responsivity. Most of the results on cryogels reported so far, however, lack a more detailed analysis to provide real conditions of the cryogelation systems. This includes the melting temperature of the gelation system, the true concentration of the monomers in the unfrozen domains, and the amounts of frozen and unfrozen water during cryogelation. We investigated here the correlations between the cryogel properties and the real conditions of cryogelation. Formation of strong polyelectrolyte PAMPS cryogels was selected for this research because of their wide range of application areas, including water purification, food industry, agriculture, energy and environmental fields, and bioengineering. Cryogelation reactions were conducted in frozen aqueous solutions of AMPS and BAAM at -18°C in the presence of a redox initiator system at -18°C . We found that the nominal AMPS concentration C_o affects significantly the porous structure of the cryogels. Both the total volume of the pores and the distance between pore channels decrease whereas the average diameter of the pores increases with increasing AMPS concentration C_o . These morphological variations depending on C_o could be explained with the local concentrations of the reaction components during cryogelation. The measurements reveal a continuous decrease of the volume of ice acting as a template

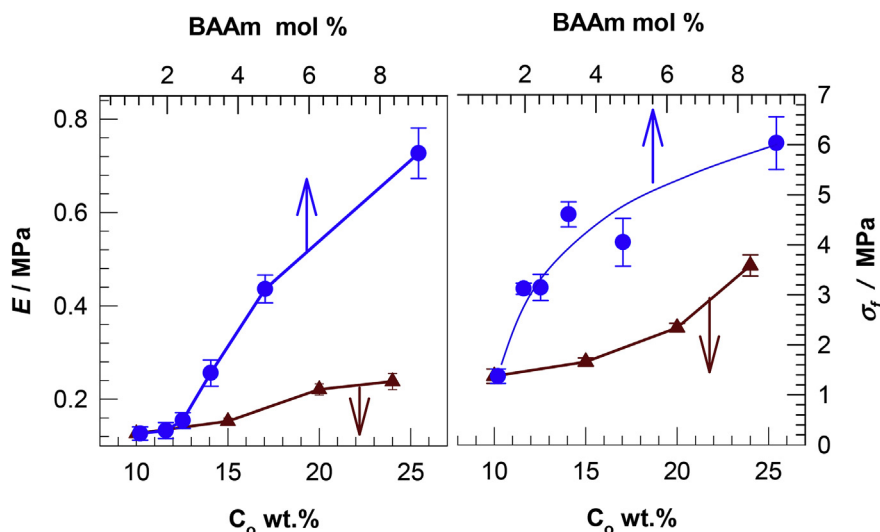


Fig. 9. Young's modulus E and compressive fracture stress σ_f of cryogels plotted against BAAM mol % (circles) and C_o wt % (triangles).

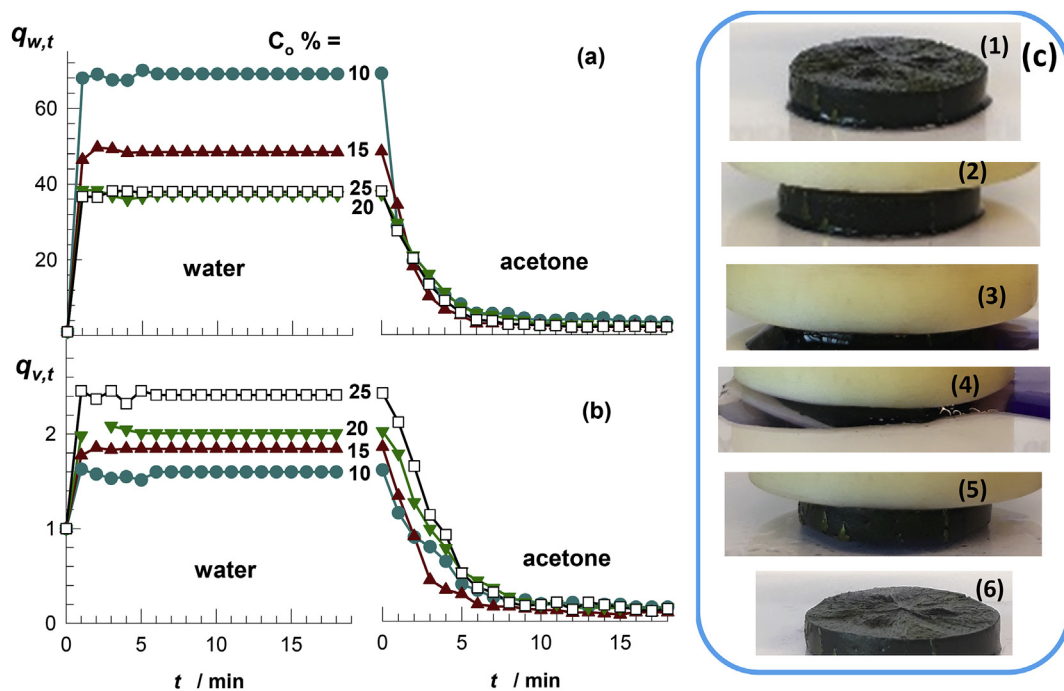


Fig. 10. (a, b): Swelling and deswelling of PAMPS cryogels in water and acetone, respectively. Weight $q_{w,t}$ (a) and volume swelling ratios $q_{v,t}$ (b) are shown as a function of contact time t . The monomer concentration C_o is indicated. BAAM = 1.2 mol %. (c): Images of a cryogel specimen under loading and unloading. The specimen was colored with a dye for clarity. $C_o = 10$ wt %. BAAM = 1.2 mol %.

for the pores in the reaction system with increasing C_o , which is in accord with the experimental results. Moreover, the melting temperature T_m of the monomer solution was found to decrease with increasing C_o . Because decreasing T_m means a slower rate of freezing of water in the reaction solution, larger ice crystals will form as C_o is increased leading to the formation of larger pores and hence, smaller spacing between the pores. Further, decreasing freezing rate of water also leads to a lesser degree of alignment of growing ice crystals, which is in accord with the experimental results. The extent of cryoconcentration was found to be the highest at the lowest monomer concentration of 10 wt %, i.e., the true concentration C_{true} of the monomers in unfrozen domains is about 2.4-fold larger than its nominal value C_o . The results also show a significant improvement in the mechanical properties of the cryogels with increasing BAAM content. PAMPS cryogels prepared at 9.1 mol % BAAM exhibit the highest modulus (0.73 ± 0.05 MPa) and could withstand up to 6.0 ± 0.5 MPa compressive fracture stress.

The results of the present study thus reveal that the following parameters of cryogelation systems determine the properties of the final cryogels:

- 1) The melting temperature T_m of the cryogelation system,
- 2) the volume of ice after cryogelation
- 3) the fraction f_{unf} of unfrozen water during cryogelation, and
- 4) the monomer concentration C_{true} in unfrozen domains.

Because these parameters are determined by DSC, such simple measurements conducted on frozen gelation solutions are means for predicting the final cryogel properties. For instance, decreasing T_m of the cryogelation system also decreases the freezing rate of the solution leading to the formation of larger pores with a lesser degree of alignment. Further, the volume of ice template after cryogelation determines the total volume of the pores. Because the unfrozen domains in the reaction system form the pore walls in the final cryogels, the monomer concentration C_{true} in these domains reflects the polymer concentration of the pore walls. Thus, a higher C_{true} means a higher polymer concentration of the pore walls and hence, a higher mechanical stability of

the porous structure of the cryogels (Fig. 7). Similarly, increasing the fraction f_{unf} of unfrozen water also increases the amount of polymer in the pore walls contributing to the mechanical strength of the cryogels.

Acknowledgments

E.S. thanks TUBITAK BIDEB for a PhD scholarship. O. O. thanks Turkish Academy of Sciences (TUBA) for the partial support.

Appendix A. Supplementary data

Supplementary data related to this article can be found at <https://doi.org/10.1016/j.polymer.2019.121603>.

References

- [1] L.W. Fisher, A.R. Sochor, J.S. Tan, Chain characteristics of poly(2-acrylamido-2-methylpropanesulfonate) polymers. 1. light-scattering and intrinsic-viscosity studies, *Macromolecules* 10 (1977) 949–954.
- [2] Z. Tong, X. Liu, Swelling equilibria and volume phase transition in hydrogels with strongly dissociating electrolytes, *Macromolecules* 27 (1994) 844–848.
- [3] X. Liu, Z. Tong, O. Hu, Swelling equilibria of hydrogels with sulfonate groups in water and in aqueous salt solutions, *Macromolecules* 28 (1995) 3813–3817.
- [4] S. Durmaz, O. Okay, Acrylamide/2-acrylamido-2-methyl propane sulfonic acid sodium salt -based hydrogels: synthesis and characterization, *Polymer* 41 (2000) 3693–3704.
- [5] N. Gundogan, D. Melekaslan, O. Okay, Rubber elasticity of poly(N-isopropylacrylamide) gels at various charge densities, *Macromolecules* 35 (2002) 5616–5622.
- [6] E. Su, O. Okay, Hybrid cross-linked poly(2-acrylamido-2-methyl-1-propanesulfonic acid) hydrogels with tunable viscoelastic, mechanical and self-healing properties, *React. Funct. Polym.* 123 (2018) 70–79.
- [7] B. Boonkaew, P.M. Barber, S. Rengpipat, P. Supaphol, M. Kempf, J. He, V.T. John, L. Cuttle, Production with gamma irradiation creates silver nanoparticles and radical polymerization, *J. Pharm. Sci.* 103 (2014) 3244–3253.
- [8] C. Yang, Z. Liu, C. Chen, K. Shi, L. Zhang, X.-J. Ju, W. Wang, R. Xie, L.Y. Chu, Reduced graphene oxide-containing smart hydrogels with excellent electro-response and mechanical properties for soft actuators, *ACS Appl. Mater. Interfaces* 9 (2017) 15758–15767.
- [9] A. Jones, D. Vaughan, Hydrogel dressings in the management of a variety of wound types: a review, *J. Orthop. Nurs.* 9 (2005) 1–11.
- [10] J.P. Gong, T. Kurokawa, T. Narita, G. Kagata, Y. Osada, G. Nishimura, M. Kinjo, Synthesis of hydrogels with extremely low surface friction, *J. Am. Chem. Soc.* 123

- (2001) 5582–5583.
- [11] K. Nalampang, R. Panjakha, R. Molloy, B.J. Tighe, Structural effects in photopolymerized sodium AMPS hydrogels crosslinked with poly(ethylene glycol) diacrylate for use as burn dressings, *J. Biomater. Sci. Polym. Ed.* 24 (2013) 1291–1304.
- [12] N. Sahiner, F. Seven, Energy and environmental usage of super porous poly(2-acrylamido-2-methyl-1-propan sulfonic acid) cryogel support, *RSC Adv.* 4 (2014) 23886–23897.
- [13] V.I. Lozinsky, Cryogels on the basis of natural and synthetic polymers: preparation, properties and application, *Russ. Chem. Rev.* 71 (2002) 489–511.
- [14] V.I. Lozinsky, Cryostructuring of polymeric systems. 50. Cryogels and cryotropic gel-formation: terms and definitions, *Gels* 4 (2018) 77.
- [15] O. Okay, V.I. Lozinsky, Synthesis and structure–property relationships of cryogels, *Adv. Polym. Sci.* 263 (2014) 103–157.
- [16] V.I. Lozinsky, O. Okay, Basic principles of cryotropic gelation, *Adv. Polym. Sci.* 263 (2014) 49–101.
- [17] S.E. Kudaibergenov, Physicochemical, complexation and catalytic properties of polyampholyte cryogels, *Gels* 5 (2019) 8.
- [18] M.M. Ozmen, O. Okay, Superfast responsive ionic hydrogels: effect of the monomer concentration, *J. Macromol. Sci. A: Pure Appl. Chem.* 43 (2006) 1215–1225.
- [19] F. Ak, Z. Oztoprak, I. Karakutuk, O. Okay, Macroporous silk fibroin cryogels, *Biomacromolecules* 14 (2013) 719–727.
- [20] A. Argun, V. Can, U. Altun, O. Okay, Non-ionic double and triple network hydrogels of high mechanical strength, *Macromolecules* 47 (2014) 6430–6440.
- [21] H. Zhang, A.I. Cooper, Aligned porous structures by directional freezing, *Adv. Mater.* 19 (2007) 1529–1533.
- [22] B. Yetiskin, O. Okay, High-strength silk fibroin scaffolds with anisotropic mechanical properties, *Polymer* 112 (2017) 61–70.
- [23] B. Yetiskin, O. Okay, High-strength and self-recoverable silk fibroin cryogels with anisotropic swelling and mechanical properties, *Int. J. Biol. Macromol.* 122 (2019) 1279–1289.